RMetS
Royal Meteorological Society

Gradient-based scales and similarity laws in the stable boundary layer

Z. Sorbjan[a,b]*
[a]*Marquette University, Milwaukee, Wisconsin, USA*
[b]*Institute of Geophysics, Polish Academy of Sciences, Warsaw, Poland*
*Correspondence to: Z. Sorbjan, Physics Dept., Marquette University, Milwaukee, WI 53201, PO Box 1181, USA.
E-mail: zbigniew.sorbjan@mu.edu

Three gradient-based scaling systems for the stably stratified boundary layer are introduced and examined by using data collected during the SHEBA field programme in the Arctic. The resulting similarity functions for fluxes and variances are expressed in an analytical form, which is expected to be essentially unaffected by self-correlation in a very stable regime. The flux Richardson number *Rf* is found to be proportional to the Richardson number *Ri*, with the proportionality coefficient varying slightly with stability, from 1.11 to 1.47. The Prandtl number decreases from 0.9 in nearly neutral conditions to 0.7 for larger values of *Ri*. The negative correlation coefficient between the vertical velocity and temperature, $-r_{w\theta}$, has a local maximum at *Ri* of about 0.08, and monotonically decreases with larger values of the Richardson number. The turbulent kinetic energy budget indicates that for $Ri > 0.7$, turbulence must be non-stationary, i.e. decaying or sporadic. Turbulence within the stably stratified boundary layer can be classified by four regimes: 'nearly neutral' ($0 < Ri < 0.02$), 'weakly stable' ($0.02 < Ri < 0.12$), 'very stable' ($0.12 < \mathrm{Ri} < 0.7$), and 'extremely stable' ($\mathrm{Ri} > 0.7$). **Copyright © 2010 Royal Meteorological Society**

Key Words: gradient-based scaling; SHEBA data; similarity theory; stable boundary layer

Received 19 August 2009; Revised 1 April 2010; Accepted 16 April 2010; Published online in Wiley InterScience 19 July 2010

Citation: Sorbjan Z. 2010. Gradient-based scales and similarity laws in the stable boundary layer. *Q. J. R. Meteorol. Soc.* **136**: 1243–1254. DOI:10.1002/qj.638

1. Introduction

The Monin–Obukhov similarity is regarded as the major tool for understanding near-surface turbulence. Since the early 1950 s, its universal framework has been systematically examined and applied in the analysis of numerous field observations. Data accumulated during recent years indicate, however, that the approach has limited utility in very stable conditions. Specifically, the similarity predictions for the gradients can be formally derived only for sub-critical conditions (e.g. Sorbjan, 2006a; 2006b), despite the observational evidence that stable turbulence survives at Richardson numbers exceeding the critical value $Ri_c \approx 0.2$ (e.g. Galperin *et al.*, 2007). Similarity scales decrease with thermal stability, causing the similarity functions to become practically singular with strongly scattered values. The definitions of the universal functions and the similarity argument z/L_* contain common divisors (u_*, T_*), a property referred to as 'self-correlation', where u_*, T_*, L_* are the Monin–Obukhov scales (see section 3.1). As a result, a relationship between the similarity functions and their argument is difficult to be established in very stable conditions with satisfactory confidence (e.g. Klipp and Mahrt, 2004; Baas *et al.*, 2006). Moreover, the definition of the stability parameter, z/L_*, includes a ratio of fluxes, which can cause ambiguities, especially when both temperature and wind fluxes are small (Grachev *et al.*, 2008). In such cases there are difficulties in differentiating between a nearly neutral state with weak velocity and very stable conditions. By replacing the argument z/L_* by the Richardson number *Ri*, the severity of the self-correlation problem can be reduced (Sorbjan, 2006b).

Copyright © 2010 Royal Meteorological Society

Some of the aforementioned problems could be resolved by defining similarity scales in terms of the moments of turbulence, which possess 'better behaviour' in very stable conditions than do the turbulent fluxes (e.g. Sorbjan, 2006a). Thus, the purpose of this paper is to further explore alternative forms of similarity scales and to examine the resulting similarity laws in the stably stratified boundary layer.

The paper has the following structure. Section 2 discusses the theoretical background in terms of the K-theory. The scaling systems and similarity functions are introduced in section 3. The empirical evaluation is presented in section 4 through the use of the experimental data collected during the SHEBA experiment. A general discussion of our work is presented in section 5. Finally, conclusions are provided in section 6.

2. Background

Let us consider a classic approach of the K-theory, which allows the expression of the turbulent fluxes of momentum $\tau = \sqrt{(-\overline{u'w'})^2 + (-\overline{v'w'})^2}$ and heat $H = \overline{w'\Theta'}$ in terms of the virtual potential temperature gradient $\Gamma = \mathrm{d}\Theta/\mathrm{d}z > 0$ and the wind shear $S = \sqrt{(\mathrm{d}U/\mathrm{d}z)^2 + (\mathrm{d}V/\mathrm{d}z)^2}$ in a stationary, horizontally homogenous, stably-stratified shear flow:

$$\tau = K_{\mathrm{m}} S \tag{1a}$$

$$H = -K_{\mathrm{h}} \Gamma \tag{1b}$$

where

$$K_{\mathrm{m}} = (\kappa z)^2 S f_{\mathrm{m}} \tag{2a}$$

$$K_{\mathrm{h}} = (\kappa z)^2 S f_{\mathrm{h}}. \tag{2b}$$

Above, the overbar indicates the ensemble averaging operator, U and V are the components of the wind velocity, f_{m} and f_{h} are empirical functions of the Richardson number, which is defined as $Ri = N^2/S^2$, $N = \sqrt{\beta\Gamma}$ is the Brunt–Väisälä frequency, $\beta = g/T_0$ is the buoyancy parameter, g is the gravity acceleration, T_0 is the reference temperature, $\kappa = 0.4$ is the von Kármán constant, and z is the height. Equation (2a) is based on the expression for eddy viscosity $K_{\mathrm{m}} = l^2 S$ of Prandtl (1932), and the mixing length $l = \kappa z/(1 + \kappa z/l_\infty)$ of Blackadar (1962), with the ratio of height and the parameter l_∞ assumed to be dependent on the Richardson number. The eddy diffusivity K_{h} is defined analogously.

We will augment the above equations by considering a simplified, steady-state, horizontally homogeneous balance of the vertical velocity variance σ_w^2 in the form (e.g. Sorbjan, 1989):

$$\tau S + \beta H \sim \sigma_w^2 \frac{\sigma_{\mathrm{w}}}{\kappa z f_\varepsilon} \tag{3}$$

where f_ε is an empirical function of the Richardson number. The left-hand side of (3) describes the shear production and the work against the buoyant force, while the right-hand side represents the dissipation rate. The diffusion and pressure terms are neglected as small in stable conditions. Following Kolmogorov (1941), the dissipation rate in (3) is parametrized as being proportional to the mixing length (the term in the denominator) and the turbulent kinetic energy. In turn, this expression can be expressed as a product of the vertical velocity variance and the anisotropy function dependent on the Richardson number. The von Kármán constant κ is added for convenience.

In addition, we will consider the simplified, steady-state, horizontally homogeneous balance of the temperature variance σ_θ^2 in the form:

$$-2H\Gamma \sim \frac{\sigma_\theta^2 \sigma_w}{\kappa z f_{\mathrm{d}}} \tag{4}$$

where f_{d} is an empirical function of the Richardson number. The left-hand side of (4) expresses the production of temperature fluctuations, and the right-hand side is the dissipation rate of the temperature variance. We neglect the diffusion term as small. The dissipation rate for the temperature fluctuations is parametrized in terms of a time-scale, which is assumed to be proportional to the mixing length and the vertical velocity variance.

When the empirical functions $f_{\mathrm{m}}, f_{\mathrm{h}}, f_\varepsilon$, and f_{d} are specified, the system (1)–(4) is closed. It describes (for given S, Γ, β and z) the relationship among the fluxes τ, H, and variances σ_w, σ_θ. We will not attempt to find the solution for the system (1)–(4). Instead, in the following section, some general conclusions about the above system will be derived by employing the approach of dimensional analysis. Such an analysis has a great tradition in meteorology and oceanography, and has been successfully applied to describe the properties of turbulence by Kolmogorov, Obukhov, Monin, Ozmidov and others (e.g. Barenblatt, 1996).

3. Scaling systems

A simple analysis of the system (1)–(4) indicates that the choice of the similarity scales for the set of eight variables: $\{\tau, H, \sigma_w, \sigma_\theta, S, \Gamma, z, \beta\}$, with three independent units, [m], [s], [K], is not unique. Thus, it can be performed in a number of ways. Generally, any three dimensionally independent parameters in the above list can be selected to build a system of three scales for length, temperature and velocity. Below, we will consider scaling systems, based on the following choice of the parameter combinations:

$$\{\tau,\ H,\ \beta\} \tag{5a}$$

$$\{\sigma_w,\ \Gamma,\ \beta\} \tag{5b}$$

$$\{\sigma_\theta,\ \Gamma,\ \beta\} \tag{5c}$$

$$\{z,\ \Gamma,\ \beta\} \tag{5d}$$

We will refer to the scales derived from the first set of parameters as 'flux-based scaling', while the remaining sets will be called the 'gradient-based scaling'. It should be mentioned that other 'gradient-based scaling' systems could also be proposed. For example, one could consider $\{\varepsilon, \Gamma, \beta\}$ as governing parameters, where ε is the dissipation rate (Sorbjan and Balsley, 2008).

3.1. *The flux-based scaling*

Historically, the first scaling system for the atmospheric boundary layer was proposed by Monin and Obukhov (1954), who employed (5a), with the surface values of fluxes

Copyright © 2010 Royal Meteorological Society

τ_0, H_0, to construct scales for length $L_* = -{\tau_0}^{3/2}/(\kappa\beta H_0)$, temperature $T_* = -H_0/u_*$, and velocity $u_* = \sqrt{\tau_0}$. Based on a dimensional analysis, Monin and Obukhov concluded that the non-dimensional products of statistical moments X in the surface layer (such as $\sigma_w, \sigma_\theta, S, \Gamma$), and the flux-based scales, are universal functions φ_x of a single dimensionless parameter z/L_*:

$$\frac{X}{U_*^a T_*^b L_*^c} = \varphi_x(z/L_*) \tag{6}$$

where the exponents a, b, c are chosen in such a way that φ_x is dimensionless. The above result conveys the so-called 'self-similarity' property, which manifests itself in the reduction of the number of independent dimensionless variables in comparison to the number of dimensional ones (e.g. Barenblatt, 1996). As a result, self-similarity substantially simplifies the description of phenomena and their experimental, analytical and computational analysis.

By using a second-order closure scheme, Nieuwstadt (1984) demonstrated that the assumption of the constancy of fluxes with height is not necessary, so that the scales in the stable boundary layer can be height-dependent (local):

$$U_*(z) = \sqrt{\tau} \tag{7a}$$

$$\vartheta_*(z) = -\frac{H}{U_*} \tag{7b}$$

$$\Lambda_*(z) = -\frac{\tau^{3/2}}{\kappa\beta H}. \tag{7c}$$

Note that a new notation is used to mark the local scales.

Sorbjan (e.g. 1986a; 1986b; 1988) argued that the functional form of universal similarity functions of the argument z/L_* and z/Λ_* is identical in stable conditions, $\varphi_x(z/L_*) = \varphi_x(z/\Lambda_*)$. As a result

$$\frac{\kappa z}{U_*} S = \varphi_{\rm m}(z/\Lambda_*) \tag{8a}$$

$$\frac{\kappa z}{\vartheta_*} \Gamma = \varphi_{\rm h}(z/\Lambda_*) \tag{8b}$$

$$\frac{s_w}{U_*} = \varphi_w(z/\Lambda_*) \tag{8c}$$

$$\frac{s_\theta}{\vartheta_*} = \varphi_\theta(z/\Lambda_*) \tag{8d}$$

Applying a definition of the Richardson number yields:

$$Ri = \frac{z}{\Lambda_*} \frac{\varphi_{\rm h}(z/\Lambda_*)}{\varphi_{\rm m}^2(z/\Lambda_*)}. \tag{9}$$

Using (9), one can formally rewrite (8) in the equivalent form:

$$\frac{\kappa z}{U_*} S = \psi_{\rm m}(Ri) \tag{10a}$$

$$\frac{\kappa z}{\vartheta_*} \Gamma = \psi_{\rm h}(Ri) \tag{10b}$$

$$\frac{\sigma_w}{U_*} = \psi_w(Ri) \tag{10c}$$

$$\frac{\sigma_\theta}{\vartheta_*} = \psi_\theta(Ri) \tag{10d}$$

where $\psi_{\rm m}$, $\psi_{\rm h}$, ψ_w, ψ_θ are the universal similarity functions of the Richardson number. The same result can be formally obtained based on (1)–(4), with $\psi_{\rm m} \sim 1/f_{\rm m}^{1/2}$, $\psi_{\rm h} \sim f_{\rm m}^{1/2}/f_{\rm h}$, $\psi_w \sim [(1 - Ri/Pr)f_\varepsilon]^{1/3}/f_{\rm m}^{1/6}$, $\psi_\theta \sim f_{\rm m}^{5/6} f_e^{1/2}/\{f_{\rm h} f_\varepsilon (1 - Ri/Pr)\}^{1/6}$, and an additional assumption that $Ri/Pr < 1$, where $Pr \equiv K_{\rm m}/K_{\rm h} = f_{\rm m}/f_{\rm h}$ is the Prandtl number. As a consequence, we conclude that the K-theory formulation (1)–(4) is equivalent to the Monin–Obukhov similarity approach.

In neutral conditions, the parameters z/Λ_* and Ri are nearly zero, which implies that the values of similarity functions are constant. Specifically, $\varphi_{\rm m}(0) = 1$ and $\varphi_{\rm h}(0) = Pr_0$, where Pr_0 is a constant, referred to as the neutral value of the Prandtl number. According to the Monin–Obukhov theory, when the temperature gradient Γ is positive and sufficiently large, turbulence is expected to be local and independent on the distance from the underlying surface (the 'z-less regime'). In this case, a dimensional analysis leads to the conclusion that the similarity functions are linear, $\varphi_{\rm m} \sim \varphi_{\rm h} \sim z/\Lambda_*$. With increasing thermal stratification, the parameter $z/\Lambda_* = \kappa z\beta\vartheta_*/U_*^2 \to 0/0$. As a result, the similarity functions become singular (large), and strongly impacted by self-correlation.

3.2. *The gradient-based σ_w - scaling*

Now, let us consider the similarity scaling based on (5b), which involves the vertical velocity variance σ_w^2, the temperature gradient Γ, and the parameter β (Sorbjan, 2006a):

$$U_w = \sigma_w \tag{11a}$$

$$T_w = \frac{N\sigma_w}{\beta} \tag{11b}$$

$$L_w = \frac{\sigma_w}{N}. \tag{11c}$$

The above scales are considered only for the case of the Brunt–Väisälä frequency N being sufficiently large. Applying (11) to (1)–(4) yields:

$$\frac{\tau}{U_w^2} = (\kappa z/L_w)^2 F_{\rm t}(Ri) \tag{12a}$$

$$-\frac{H}{U_w T_w} = (\kappa z/L_w)^2 F_{\rm h}(Ri) \tag{12b}$$

$$\frac{\sigma_\theta}{T_w} = (\kappa z/L_w) F_\theta(Ri) \tag{12c}$$

where $F_{\rm t} = f_{\rm m}/Ri$, $F_{\rm h} = f_{\rm h}/Ri^{1/2}$, $F_\theta = f_d^{1/2}\, f_{\rm h}^{1/2}/\{f_{\rm m} f_\varepsilon (1 - Ri/Pr)\}^{1/6}$, and $Ri/Pr < 1$.

Equation (3) implies that

$$\frac{L_w}{\kappa z} = \Phi_w(Ri) \tag{13}$$

where $\Phi_w(Ri) \sim \{f_{\rm m} f_\varepsilon (1 - Ri/Pr)\}^{1/3}/Ri^{1/2}$ can be seen to be a function of the Richardson number. Using (13), equations (12a)–(12c) can be rewritten in an equivalent form:

$$\frac{\tau}{U_w^2} = \Phi_{\rm t}(Ri) \tag{14a}$$

Copyright © 2010 Royal Meteorological Society

$$-\frac{H}{U_w T_w} = \Phi_{\rm h}(Ri) \tag{14b}$$

$$\frac{\sigma_\theta}{T_w} = \Phi_\theta(Ri) \tag{14c}$$

where $\Phi_{\rm m}$, $\Phi_{\rm h}$, and Φ_θ are universal functions of the Richardson number. Since the above expressions were derived based on the K-theory formulation (1)–(4), and we have found to be equivalent to the Monin–Obukhov similarity approach, we can conclude that (13)–(14) is also formally equivalent to the Monin–Obukhov similarity theory. An analogous result can also be derived by using second-order closure equations (Sorbjan, 2006a).

Using dimensional analysis, (14) can be generalized by asserting that the non-dimensional products of statistical moments X in the surface layer and the scales (11), are expected to be universal functions Φ_x of a single dimensionless parameter Ri:

$$\frac{X}{U_w^a T_w^b L_w^c} = \Phi_x(Ri) \tag{15}$$

3.3. The gradient-based σ_θ scaling

Yet another similarity scaling can be introduced based on (5c). It involves the temperature variance σ_θ^2 and the Brunt–Väisälä frequency N:

$$U_\theta = \frac{\beta\sigma_\theta}{N} \tag{16a}$$

$$T_\theta = \sigma_\theta \tag{16b}$$

$$L_\theta = \frac{\beta\sigma_\theta}{N^2}, \tag{16c}$$

where the Brunt–Väisälä frequency N is assumed to be sufficiently large.

Applying (16) to (1)–(4) yields:

$$\frac{\tau}{U_\theta^2} = (\kappa z/L_\theta)^2 F_{\rm t}(Ri) \tag{17a}$$

$$-\frac{H}{U_\theta T_\theta} = (\kappa z/L_\theta)^2 F_{\rm h}(Ri) \tag{17b}$$

$$\frac{\sigma_w}{U_\theta} = (\kappa z/L_\theta) F_w(Ri) \tag{17c}$$

$$\frac{L_\theta}{\kappa z} = \Psi_\theta(Ri) \tag{17d}$$

where $F_w \sim [f_{\rm m} f_\varepsilon(1 - Ri/Pr)]^{1/3}/Ri^{1/2}$, $\Psi_\theta \sim (f_d f_h)^{1/2}/[f_m f_\varepsilon(1 - Ri/Pr)]^{1/6}$, and $Ri/Pr < 1$.

Using (17d), we obtain from (17a)–(17c):

$$\frac{\tau}{U_\theta^2} = \Psi_{\rm t}(Ri) \tag{18a}$$

$$-\frac{H}{U_\theta T_\theta} = \Psi_{\rm h}(Ri) \tag{18b}$$

$$\frac{\sigma_w}{U_\theta} = \Psi_w(Ri). \tag{18c}$$

It can be noted that $\Psi_w \equiv 1/\Phi_\theta$.

Again employing a dimensional analysis, we can generalize (18) by stating that the non-dimensional products of statistical moments X in the surface layer and the above scales are expected to be universal functions Ψ_x of a single dimensionless parameter Ri:

$$\frac{X}{U_\theta^a T_\theta^b L_\theta^c} = \Psi_x(Ri) \tag{19}$$

3.4. The gradient-based master scaling

An alternative similarity scaling can be introduced by using (5d), which involves the temperature gradient Γ, the buoyancy parameter β and height z:

$$U_s = \kappa\, z\, N \tag{20a}$$

$$T_s = \kappa\, z\Gamma \tag{20b}$$

$$L_s = \kappa\, z, \tag{20c}$$

where κ the von Kármán constant was added for convenience. As before, we will consider only cases when the Brunt–Väisälä frequency N is sufficiently large. We will refer to (20a, b, c) as master scaling.

Employing (20), we obtain from (1)–(4):

$$\frac{\tau}{U_s^2} = G_{\rm t}(Ri) \tag{21a}$$

$$-\frac{H}{U_s T_s} = G_{\rm h}(Ri) \tag{21b}$$

$$\frac{\sigma_w}{U_s} = G_w(Ri) \tag{21c}$$

$$\frac{\sigma_\theta}{T_s} = G_\theta(Ri) \tag{21d}$$

where $G_t \sim f_m/Ri$, $G_{\rm h} = f_h/Ri^{1/2}$, $G_w \sim [f_m f_\varepsilon(1 - Ri/Pr)]^{1/3}/Ri^{1/2}$, $G_\theta \sim (f_d f_h)^{1/2}/[f_m f_\varepsilon/(1 - Ri/Pr)]^{1/6}$, and $Ri/Pr < 1$. It can be noted that $G_t \equiv F_t$, $G_h \equiv F_h$, $G_w \equiv \Phi_w$, $G_\theta \equiv \Psi_\theta$.

Analogous to the previous scaling cases, we can generalize the above system by stating that the non-dimensional products of statistical moments X in the surface layer and the above scales must be universal functions of a single dimensionless parameter Ri:

$$\frac{X}{U_s^a T_s^b L_s^c} = G_x(Ri) \tag{22}$$

Note that the temperature gradient Γ appears on both sides of (22), within the similarity scales and in the definition of the Richardson number. This fact implies self-correlation, due to errors in the evaluation of Γ. However, it is reasonable to expect that such errors are relatively small when the

Copyright © 2010 Royal Meteorological Society

temperature gradient is sufficiently large, and thus the self-correlations effects related to Γ do not represent a serious issue.

The considered gradient-based and flux-based scaling systems are related. Based on (11), (16) and (20) one can obtain:

$$\frac{U_w}{U_s} = \frac{T_w}{T_s} = \frac{L_w}{L_s} = G_w \tag{23a}$$

$$\frac{U_\theta}{U_s} = \frac{T_\theta}{T_s} = \frac{L_\theta}{L_s} = G_\theta \tag{23b}$$

$$\frac{U_\theta}{U_w} = \frac{T_\theta}{T_w} = \frac{L_\theta}{L_s} \tag{23c}$$

$$\frac{U_*}{U_s} = \frac{T_s}{T_*} G_\mathrm{h} = \frac{L_*}{\kappa L_s} \frac{G_\mathrm{h}}{G_\mathrm{t}} = G_\mathrm{t}^{1/2} \tag{23d}$$

By employing (10a), (10b), and (23d), one can also obtain the relationship between the Monin–Obukhov and gradient-based functions:

$$G_\mathrm{t} = \frac{1}{Ri\psi_\mathrm{m}{}^2} \tag{24a}$$

$$G_\mathrm{h} = \frac{1}{Ri^{1/2}\psi_\mathrm{m}\psi_\mathrm{h}} \tag{24b}$$

The master scaling does not involve any higher order moments. Because of dependence only on gradients, its application seems to be the most advantageous. Using the master-scaling similarity functions, all other similarity functions can also be derived.

4. Empirical evaluation

4.1. Data

The similarity functions formulated in the previous section will now be examined using the data collected during the Surface Heat Budget of the Arctic Ocean (SHEBA) experiment. Detailed overviews of the SHEBA programme and its data can be found in the papers of Andreas *et al.* (1999; 2003; 2006), Persson *et al.* (2002) and Grachev *et al.* (2005; 2007a; 2007b; 2008). Thus, herein, only brief information about SHEBA instruments and data will be provided.

The experiment took place over Arctic pack ice, drifting in the Beaufort Gyre to the north of Alaska (latitude from 74°N to 81°N), from October 1997 through to September 1998. The sub-polar site offered a number of advantages, especially due to the stationarity of weather conditions, and the lack of contamination by drainage or strong advective flows. Except for rare periods, instruments ran almost continuously for 11 months and produced well over 6000 hours of useful data, covering a wide range of stability conditions.

Turbulent and mean meteorological data during SHEBA were obtained on the 20 m main tower (Grachev *et al.*, 2005). Observations were continuously collected at five levels, located at 2.2 m, 3.2 m, 5.1 m, 8.9 m, and 18.2 or 14 m above the surface. The variances and covariances at each level were based on one-hour averaging, and derived through frequency integration of both spectra and cospectra. To prevent a possible flux loss caused by inadequate frequency responses and sensor separations, a prerequisite that the wind velocity $U > 1$ m/s has been imposed on the sample. Data for the first level, which reflected a relatively large scatter due to local surface effects, were not considered. In addition, data with a temperature difference between the air at median level and the snow surface of less than 0.5°C were excluded to avoid the large uncertainty in determining the sensible heat flux. Vertical gradients of the mean wind speed and the potential temperature were obtained by fitting a second-order polynomial through the 1-hour profiles followed by an evaluation of the derivative with respect to z for levels 1–5.

The data points presented in this paper are based on a bin-averaging of the individual one-hour data at levels 2, 3, 4 and 5. For this purpose, data were first sorted into bins by using the Richardson number Ri as the sorting parameter. Then, the mean values of relevant parameters were computed for each bin (e.g. Grachev *et al.*, 2008).

It can be noted that in practice there is often a problem with the differentiation between nearly neutral and very stable regimes in cases when both temperature and wind gradients are small. The number of outliers with high values of Ri in nearly neutral conditions is often comparable with the number of points that truly have high values of Ri in very stable conditions. As a result, the Ri-outliers from the nearly neutral range can significantly distort the picture in the very stable regime. To resolve this problem, a special prerequisite was applied to data in order to limit the influence of outliers on the bin-averaging: $0.5Ri_e < Ri < 2Ri_e$, where the value of the Richardson number Ri_e was estimated based on an equation analogous to (9), with the analytical form of the Monin–Obukhov similarity functions φ_h and φ_m of z/L_* obtained by Grachev *et al. (2007*a), and Grachev *et al.* (2008). More specifically, if the actual value of a Richardson number $Ri = N^2/S^2$ was not in the range defined by Ri_e, the data point was rejected. Ultimately, this procedure removed those cases for which there was an inconsistency between the Richardson number calculated directly and analytically.

4.2. The master scaling

The dependence of the dimensionless fluxes, $G_\mathrm{t} = \tau/U_s^2$ and $G_\mathrm{h} = -H/(U_s T_s)$ on the Richardson number Ri is shown in Figure 1. The dimensionless moments $G_w = \sigma_w/U_s$ and $G_\theta = \sigma_\theta/T_s$ are depicted in Figure 2. A clustering of data points in the figures is caused by the fact that the Richardson number Ri is a sorting parameter. The vertical lines with horizontal bars represent the confidence intervals, obtained by perturbing the mean values evaluated at level 5 by one standard deviation. Because the ordinate is logarithmic, the confidence intervals are asymmetric.

The scatter in Figure 1(b) is larger than that in Figure 1(a). This can be associated with thermal inhomogeneity around the observational site (e.g. Kukharets and Tsvang, 1998; Tsvang *et al.*, 1998). The ice floe around the main tower was multi-year pack ice, with varying degrees of thickness and a heterogeneous surface of a different type and salinity, snow with a different depth and age, melt-ponds, and even leads (e.g. Sorbjan and Grachev, 2010). The various surface 'patches' were characterized by different albedo, thermal capacity and conductivity and, therefore, by different temperatures. Andreas *et al.* (1998) reported analogous behaviour for the case of humidity statistics over a surface with vegetation that was 'patchy' at metre scales.

Copyright © 2010 Royal Meteorological Society

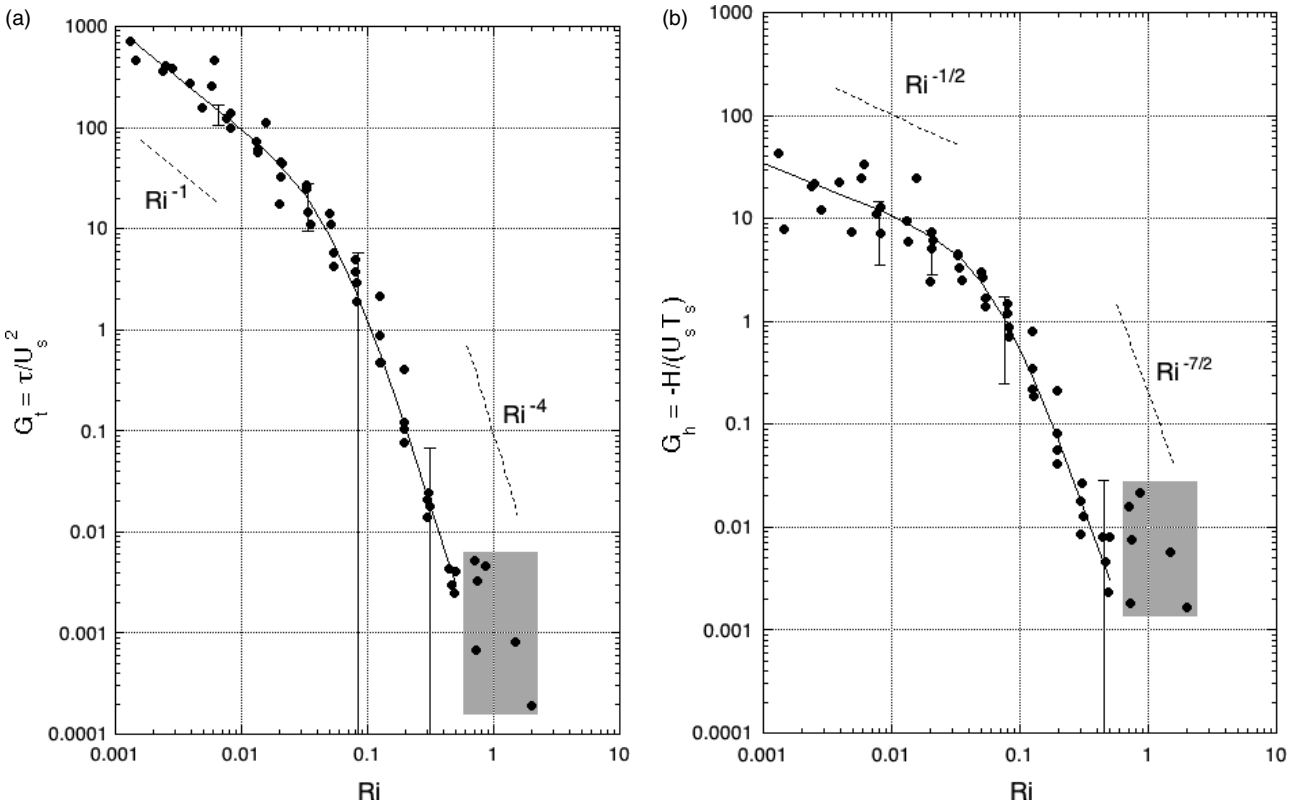

Figure 1. Dependence of the bin-averaged values of the dimensionless (a) momentum flux $G_t = \tau/U_s^2$, (b) heat flux $G_h = -H/(U_s T_s)$, on the Richardson number *Ri*. The solid lines are plotted based on Eqs. (27a) and (27b). The vertical lines represent the confidence intervals evaluated at level 5. Data points within the extremely-stable domain are marked by the shaded box.

In order to further evaluate the presented results, we note that in nearly neutral conditions, the functions f_m, f_h, f_ε, f_d are constant, and that following from (1)–(4) $\tau \sim (\kappa z S)^2$, $\sigma_w \sim \kappa z S$, and also $H \sim (\kappa z)^2 S N^2/\beta$, $\sigma_\theta \sim \kappa z N^2/\beta$. Combining these relations with (20)–(21) and (23)–(24), we can conclude that for nearly neutral conditions

$$G_t \sim Ri^{-1} \tag{25a}$$

$$G_h \sim Ri^{-1/2} \tag{25b}$$

$$G_w \sim Ri^{-1/2} \tag{25c}$$

$$G_\theta \sim Ri^{0} \tag{25d}$$

Figures 1(a), 1(b) and 2(a) confirm the above predictions for $Ri < 0.01$. However, the values of the dimensionless temperature variance G_θ in Figure 2(b) are larger than expected in the nearly neutral range. This fact implies that the values of the temperature variance are overestimated for these conditions. Analogous effects can be observed in all of the figures that involve the temperature variance.

In the supercritical range, $Ri > Ri_{cr}$, the values of the similarity functions in Figures 1 and 2 fall off in a coherent fashion with the increasing values of *Ri*. This indicates the presence of a self-similar regime in very stable conditions. Unfortunately, the dimensional analyses do not allow for the formulation of any constructive similarity prediction. Therefore, we will assume, based on the presented empirical evidence, that the similarity functions obey the following power laws:

$$G_t \sim Ri^{-4} \tag{26a}$$

$$G_h \sim Ri^{-7/2} \tag{26b}$$

$$G_w \sim Ri^{-3/2} \tag{26c}$$

$$G_\theta \sim Ri^{-1} \tag{26d}$$

with a validity range of approximately $0.1 < Ri < 0.7$. Above this range, the values of the similarity functions are incoherent and scattered. Such behaviour suggests a lack of any general similarity laws for these values of *Ri*. Consequently, we will limit our analysis to the range $Ri < 0.7$, and disregard the domain marked by the shaded boxes in Figures 1–2 (and also in the remaining figures).

Taking (25) and (26) into consideration, we adopt the following approximations of the similarity functions:

$$G_t \equiv \frac{\tau}{U_s^2} = \frac{1}{Ri(1+300Ri^2)^{3/2}} \tag{27a}$$

$$G_h \equiv -\frac{H}{U_s T_s} = \frac{1}{0.9Ri^{1/2}(1+250Ri^2)^{3/2}} \tag{27b}$$

$$G_w \equiv \frac{\sigma_w}{U_s} = \frac{1}{0.85Ri^{1/2}(1+450Ri^2)^{1/2}} \tag{27c}$$

$$G_\theta \equiv \frac{\sigma_\theta}{T_s} = \frac{5}{(1+2500Ri^2)^{1/2}}. \tag{27d}$$

The above equations are represented in Figures 1 and 2 by solid curves. The agreement of the curves with data points is generally good.

Copyright © 2010 Royal Meteorological Society

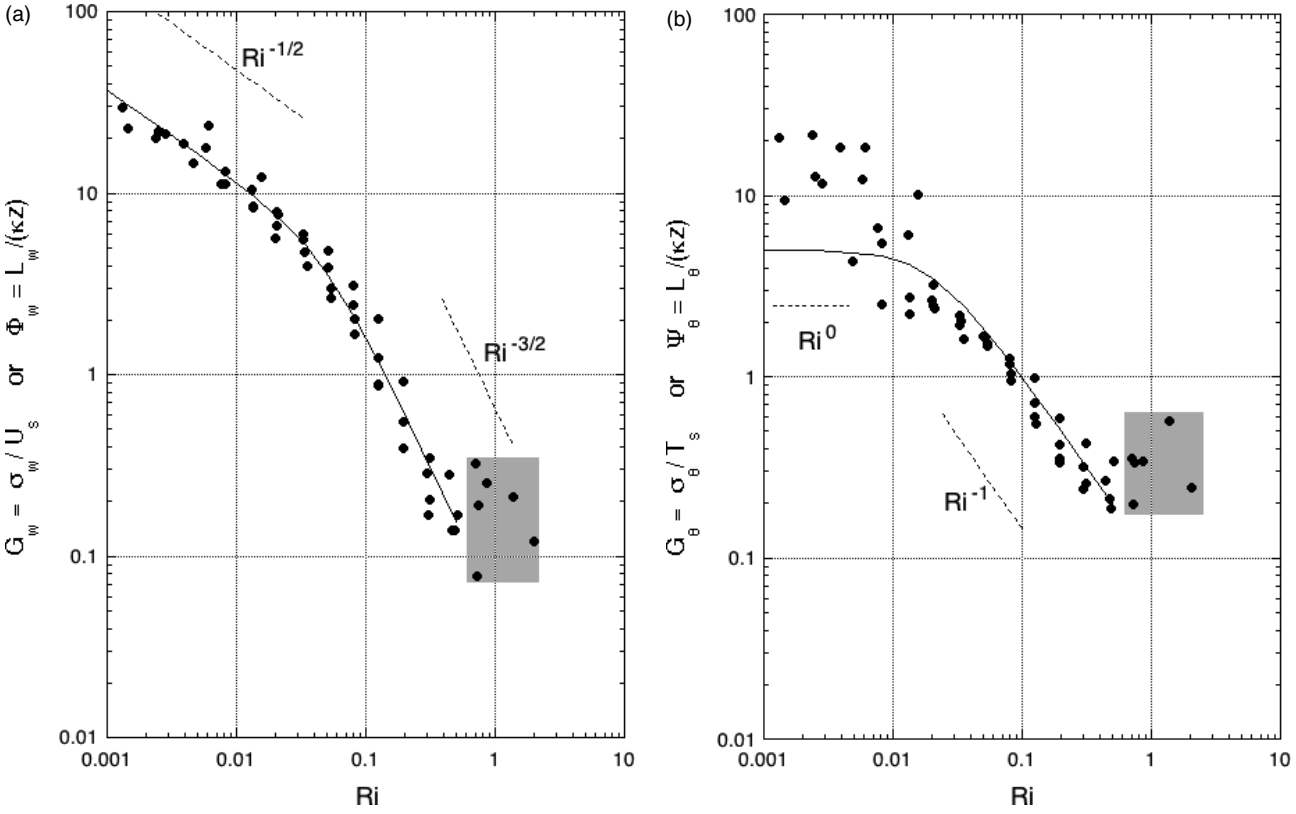

Figure 2. Dependence of the bin-averaged values of the dimensionless standard deviations for (a) vertical velocity $G_w = \sigma_w/U_s [\equiv \Phi_w = L_w/(\kappa z)]$, (b) temperature $G_\theta = \sigma_\theta/T_s$ $[\equiv \Psi_\theta = L_\theta/(\kappa z)]$, on the Richardson number *Ri*. The solid lines are plotted based on Eqs. (27c) and (27d). Data points within the extremely stable domain are marked by the shaded box.

Using (24a, b) and (27a, b), we also obtain:

$$\psi_{\rm m} \equiv \frac{\kappa z}{U_*} S = \frac{1}{Ri^{1/2} G_t^{1/2}} = (1 + 300 Ri^2)^{3/4} \qquad (28a)$$

$$\psi_{\rm h} \equiv \frac{\kappa z}{\vartheta_*} \Gamma = \frac{G_{\rm t}^{1/2}}{G_{\rm h}} = 0.9 \frac{(1 + 250 Ri^2)^{3/2}}{(1 + 300 Ri^2)^{3/4}}. \qquad (28b)$$

Further examination of the flux-based similarity functions (28) may be found in the work of Sorbjan and Grachev (2010), who used data collected during both the SHEBA and the CASES-99 field programmes.

4.3. *The σ_w-scaling*

Employing (14), (23) and (27) yields:

$$\Phi_{\rm t} \equiv \frac{\tau}{U_w^2} = G_{\rm t}/G_w^2 = 0.72 \frac{(1 + 450 Ri^2)}{(1 + 300 Ri^2)^{3/2}} \qquad (29a)$$

$$\Phi_{\rm h} \equiv -\frac{H}{U_w T_w} = G_{\rm h}/G_w^2 = 0.80\, Ri^{1/2} \frac{(1 + 450 Ri^2)}{(1 + 250 Ri^2)^{3/2}} \qquad (29b)$$

$$\Phi_\theta \equiv \frac{\sigma_\theta}{T_w} = G_\theta/G_w = 4.25\, Ri^{1/2} \frac{(1 + 450 Ri^2)^{1/2}}{(1 + 2500 Ri^2)^{1/2}} \qquad (29c)$$

The dependence of the dimensionless fluxes, $\Phi_{\rm t}$ and $\Phi_{\rm h}$, on the Richardson number *Ri* is shown in Figure 3(a) and (b).

Figure 3(a) indicates that the dimensionless momentum flux $\Phi_{\rm t}$ is constant for $Ri < 0.03$, slightly decreases in the range of *Ri* from 0.03 to 0.1, and more quickly falls off for $Ri > 0.1$. The dimensionless temperature flux $\Phi_{\rm h}$ in Figure 3(b) increases with an increasing Richardson number in near-neutral conditions, and decreases for larger values of *Ri*. At the value of *Ri* about 0.125, the negative dimensionless flux reaches a maximum, equal to about 0.27. Taking into consideration that the dimensionless flux Figure 1(b) is monotonic, this result may appear surprising. However, further analysis indicates that the result is caused by the inclusion of σ_w in the definition of the velocity and temperature scales.

4.4. *The σ_θ-scaling*

Considering (18), (23) and (27), we obtain:

$$\Psi_{\rm t}(Ri) \equiv \frac{\tau}{U_\theta^2} = G_{\rm t}/G_\theta^2 = 0.04 \frac{(1 + 2500 Ri^2)}{Ri(1 + 300 Ri^2)^{3/2}} \qquad (30a)$$

$$\Psi_{\rm h}(Ri) \equiv -\frac{H}{U_\theta T_\theta} = G_{\rm h}/G_\theta^2 = 0.044 \frac{(1 + 2500 Ri^2)}{Ri^{1/2}(1 + 250 Ri^2)^{3/2}} \qquad (30b)$$

$$\Psi_w(Ri) \equiv \frac{\sigma_w}{U_\theta} = G_w/G_\theta^2 = 0.24 \frac{(1 + 2500 Ri^2)^{1/2}}{Ri^{1/2}(1 + 450 Ri^2)^{1/2}} \qquad (30c)$$

The dependence of the dimensionless fluxes, $\Psi_{\rm t}$ and $-\Psi_{\rm h}$, on the Richardson number *Ri*, is depicted in Figure 4(a) and

Copyright © 2010 Royal Meteorological Society

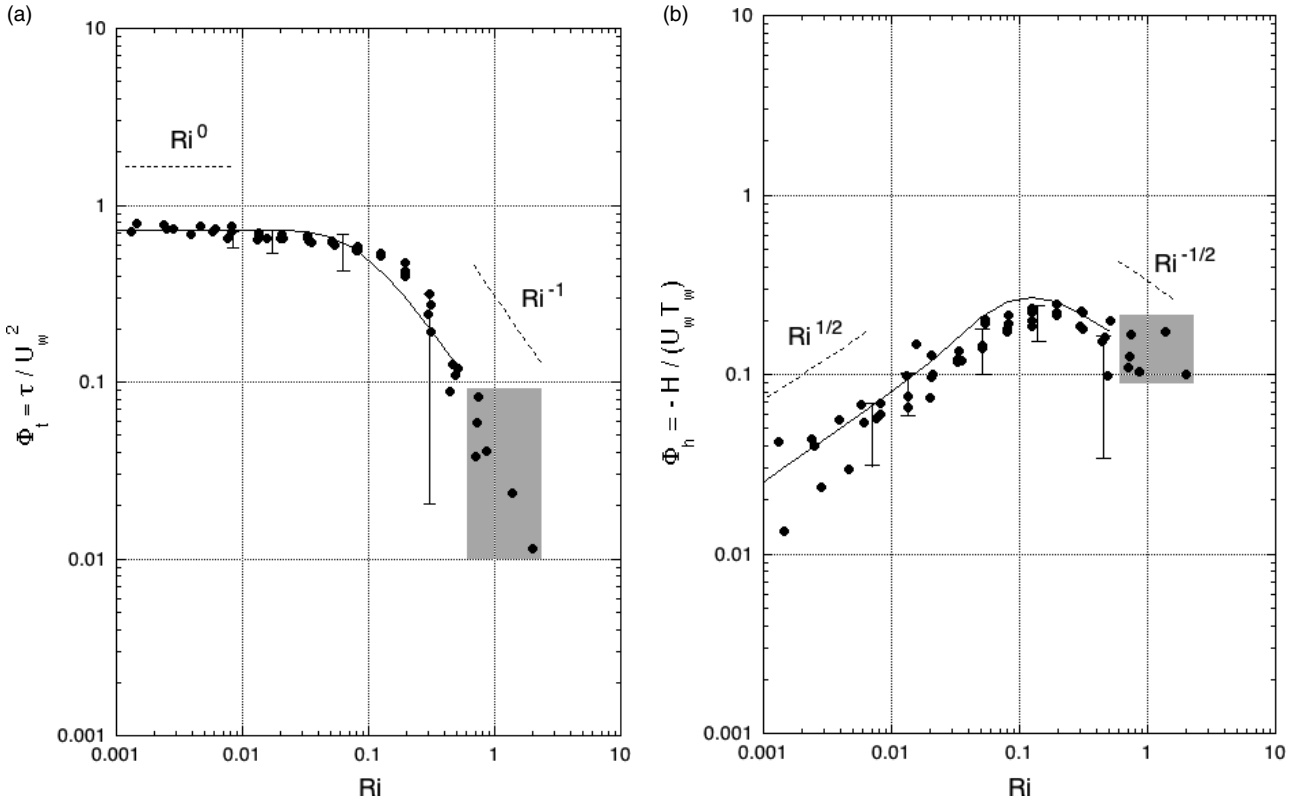

Figure 3. Dependence of the bin-averaged values of the dimensionless fluxes for (a) momentum $\Phi_t = \tau/U_w^2$, and (b) heat $\Phi_h = -H/(U_w T_w)$, on the Richardson number *Ri*. The solid lines are plotted based on Eqs. (29a) and (29b). The vertical lines represent the confidence intervals evaluated at level 5. Data points within the extremely stable domain are marked by the shaded box.

(b). The ordinate is in the range from 0.005 to 10. This range is smaller than in the previous figures, as data points for the smallest values of the Richardson number were excluded due to their significant scatter.

The scatter of data points in Figure 4(a) and (b) allows for only a tentative evaluation of the above expressions in the nearly neutral range. Equation (30a), plotted in Figure 4(a), has an inflection point around $Ri = 0.025$. Figure 4(b) shows that expression (30b) possesses a local minimum at about $Ri = 0.013$, and a local maximum at about $Ri = 0.05$. For larger values of *Ri*, the dimensionless momentum and heat fluxes monotonically decrease with an increasing *Ri*.

5. Discussion

All of the gradient-based scaling systems that were considered in this paper are formally equivalent to each other, as well as to the Monin–Obukhov similarity approach in the stable case. There exists, however, an essential difference between the flux-based approach and the gradient-based formulations. The flux-based methodology employs fluxes as external (specified) parameters. As a result, the practical application of the flux-based expressions requires inverting the similarity laws, and calculating surface fluxes from the provided (measured) values of gradients in the surface layer. This procedure is ill-posed in very stable conditions due to the small values of the flux quantities. Moreover, the effective use of the local similarity formulation (8) requires that the fluxes be known *a priori* as functions of height; often quite difficult to accomplish.

Within the gradient-based formulation, the gradients themselves play the role of external parameters and avoid the implied singularities associated with the fluxes. The gradient value can be provided from measurements, or via the use of the differential equations for momentum and heat (with appropriate boundary conditions). As a result, the cross-isobar angle and the depth of the boundary layer, which are otherwise absent in the presented similarity formulations, can be taken into consideration.

Let us consider the flux Richardson number $Rf = -\beta H/(\tau S)$. Employing (21a, b) and (27a, b), we obtain:

$$Rf = \frac{G_h}{G_t} Ri^{1/2} = \frac{Ri}{0.9} \frac{(1 + 300Ri^2)^{3/2}}{(1 + 250Ri^2)^{3/2}}. \qquad (31)$$

The above expression is illustrated in Figure 5 as a solid curve. In accordance with (31), $Rf = 1.11\ Ri$ in nearly neutral conditions, and $Rf = 1.46\ Ri$ for large values of *Ri*. Consequently, the curve in the figure only slightly differs from a straight line.

Taking into consideration that $Rf \equiv Ri/\,\mathrm{Pr}$ and by using (31), we find that

$$\mathrm{Pr} = 0.9 \frac{(1 + 250Ri^2)^{3/2}}{(1 + 300Ri^2)^{3/2}} \qquad (32)$$

Equation (32) indicates that Prandtl number is 0.9 in nearly neutral conditions, and 0.7 for larger values of *Ri*. According to Ohya (2001), Grachev *et al.* (2007b), Esau and Grachev (2007), Zilitinkevich *et al.* (2007) and Anderson (2009), the Prandtl number increases with *Ri* in supercritical conditions. However, the detailed analysis of Grachev *et al.* (2007b) implies that such a result is spurious. When one does not employ the outlier rejection discussed in section 4.1, the resulting SHEBA data do indeed show that *Pr*

Copyright © 2010 Royal Meteorological Society

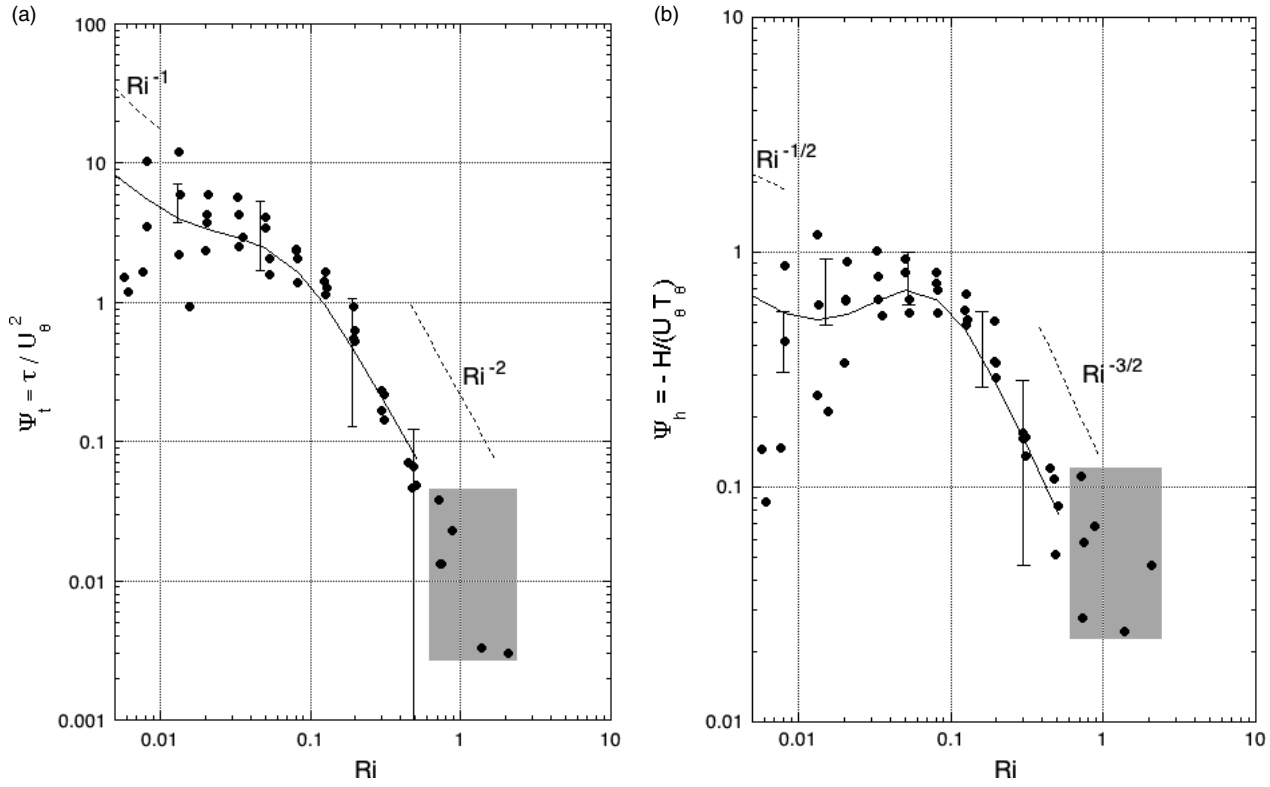

Figure 4. Dependence of the bin-averaged values of the dimensionless (a) momentum flux $\Psi_t = \tau/U_\theta^2$, and (b) heat flux $\Psi_h = -H/(U_\theta T_\theta)$, on the Richardson number *Ri*. The solid lines are plotted based on Eqs. (30a) and (30b). The vertical lines represent the confidence intervals evaluated at level 5. Data points within the extremely stable domain are marked by the shaded box.

increases with the increasing values of *Ri*. Conversely, when the outliers are not included, the Prandtl number decreases slightly, as discussed by Sorbjan and Grachev (2010).

Note that the steady-state, turbulent energy budget (3) can also be expressed in the following form:

$$K_m S^2 (1 - Rf) = \varepsilon \tag{33}$$

Since the dissipation rate ε is positive-definite, (33) allows us to conclude that the steady state, which results from the balance of shear production and buoyant-dissipative destruction, takes place only for $Rf < 1$. As seen in Figure 5, $Rf = 1$ at $Ri = 0.7$. Thus, for Richardson numbers exceeding the value $Ri_s = 0.7$, steady-state turbulence would not be present. In other words, at $Ri > R_s$, turbulence is non-stationary, i.e. decaying or sporadic. The inequality $Ri < R_s = 0.7$ is a necessary condition for the presence of steady-state turbulence. It must be satisfied for steady-state turbulence to take place.

Taking (27) into consideration, we derive the negative correlation coefficient:

$$-r_{w\theta} \equiv -\frac{H}{\sigma_w \sigma_\theta} = \frac{G_h}{G_w G_\theta} = 0.2(1 + 2500Ri^2)^{1/2} \frac{(1 + 450Ri^2)^{1/2}}{(1 + 250Ri^2)^{3/2}} \tag{34}$$

The values of $-r_{w\theta}$ are depicted in Figure 6. The ordinate in the plots spans the range from 0.005 to 10. We exclude data points for the smallest values of the Richardson number due to their significant scatter. The solid line based on (34) agrees with observations. It implies that the coefficient $-r_{w\theta}$ tends to a constant value of 0.2 in the near-neutral regime, reaches a local maximum of about 0.39 at about $Ri = 0.08$, and monotonically decreases for larger values of *Ri*.

Figure 7 depicts the dimensionless components of the doubled turbulent kinetic energy: $A_u = \sigma_u^2/q^2$, $A_v = \sigma_v^2/q^2$, $A_w = \sigma_w^2/q^2$, where σ_u^2, σ_v^2, σ_w^2 are the velocity variances, and q^2 is the doubled turbulent kinetic energy. The figure indicates that for nearly neutral conditions, all the components are approximately constant, and $A_u \approx 0.62$, $A_v \approx 0.26$, and $A_w \approx 0.12$. In the range $0.01 < Ri < 0.1$, A_u decreases to 0.5, and is approximately constant up to $Ri = 0.7$. The component A_v increases to about 0.4 at $Ri = 0.7$. Consequently, one can observe that A_u and A_v have a tendency to become nearly equal at $Ri > 0.7$. The vertical component A_w increases and reaches maximum at $Ri = 0.1$. Subsequently, it decreases for larger *Ri*. The vanishing values of A_w at larger values of *Ri* can be interpreted as the rising of an extremely stable–sporadic regime, in which turbulence becomes horizontal and concentrated in vertically uniform layers.

Referring now to the ensemble of Figures 1–6, one can identify four sub-regimes in the stable boundary layer. As shown in Figure 8, they can be listed in the following order: nearly neutral ($Ri < 0.02$), stable ($0.02 < Ri \leq 0.12$), very stable ($0.12 < Ri < 0.7$) and extremely stable ($Ri > 0.7$). In the nearly neutral regime, the master similarity functions follow the power laws (25). The stable regime is the transition between nearly neutral and very stable conditions. In the very stable regime, the master similarity functions are described by the empirical power laws (26). The potential generality of any scaling laws in the extremely stable conditions is doubtful. Figure 8 shows that when the wind shear *S* increases, turbulence becomes stronger and the turbulent regime less stable. On the other hand, when the

Copyright © 2010 Royal Meteorological Society

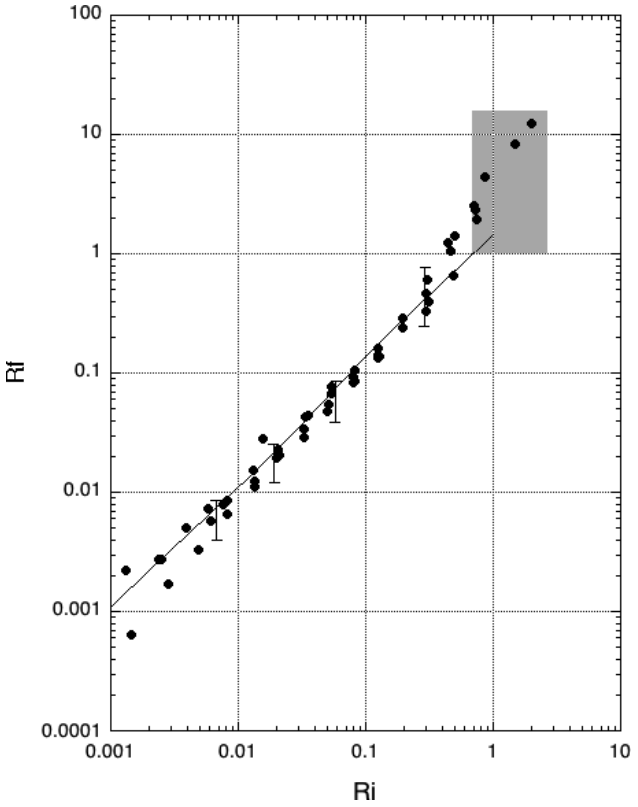

Figure 5. Dependence of the bin-averaged values of the flux Richardson number *Rf* on the gradient Richardson number *Ri*. The solid line is plotted based on Eq. (31). The vertical lines represent the confidence intervals evaluated at level 5. Data points within the extremely stable domain are marked by the shaded box.

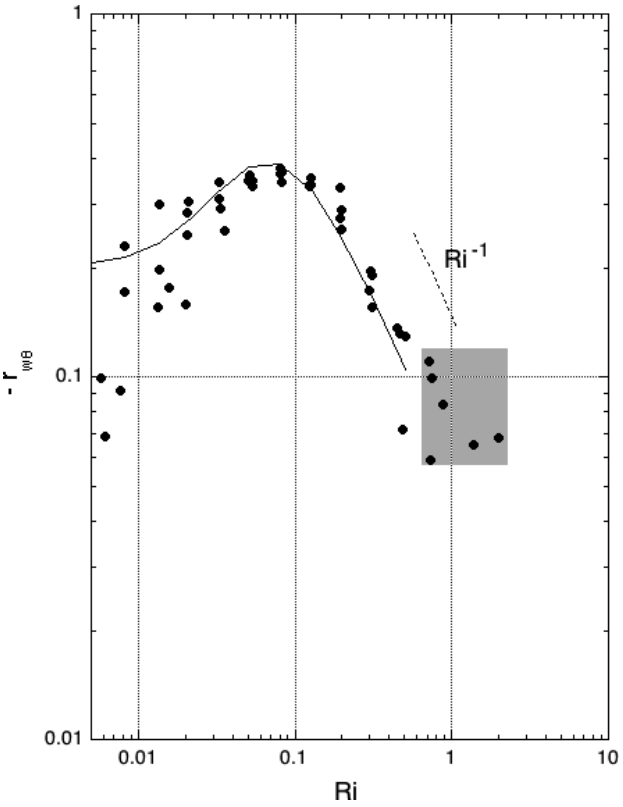

Figure 6. Dependence of the bin-averaged values of the negative correlation coefficient $-r_{w\theta}$ on the Richardson number *Ri*. The solid line is plotted based on Eq. (34). Data points within the extremely stable domain are marked by the shaded box.

Brunt–Väisälä frequency N increases, turbulence weakens and the turbulent regime becomes more stable.

6. Conclusions

Properties of the stably stratified boundary layer have been examined through the use of a gradient-based similarity approach. This formulation is formally equivalent to the Monin–Obukhov similarity approach, but possesses improved properties in very stable conditions. Specifically, it avoids the singularity imposed by small values of scales and, therefore, is less affected by self-correlation. While the Monin–Obukhov similarity scales are based on two second-order moments (momentum and heat flux), each of the variance-gradient-based scaling systems is defined through a single second-order moment (temperature or the vertical velocity variance). The master scaling formulation does not employ second-order moments, and thus its application is most advantageous.

The gradient-based similarity functions for fluxes and variances have been evaluated by using tower data collected during the SHEBA field programme. We found that the derived analytical expressions for the similarity functions are consistent with these data. The analytical expressions for the similarity functions that are conveyed in terms of the σ_w and σ_θ scales can be derived from the master scale similarity functions.

The flux Richardson number *Rf* is found to be proportional to the Richardson number, with the proportionality coefficient varying slightly with stability, from 1.11 to 1.47.

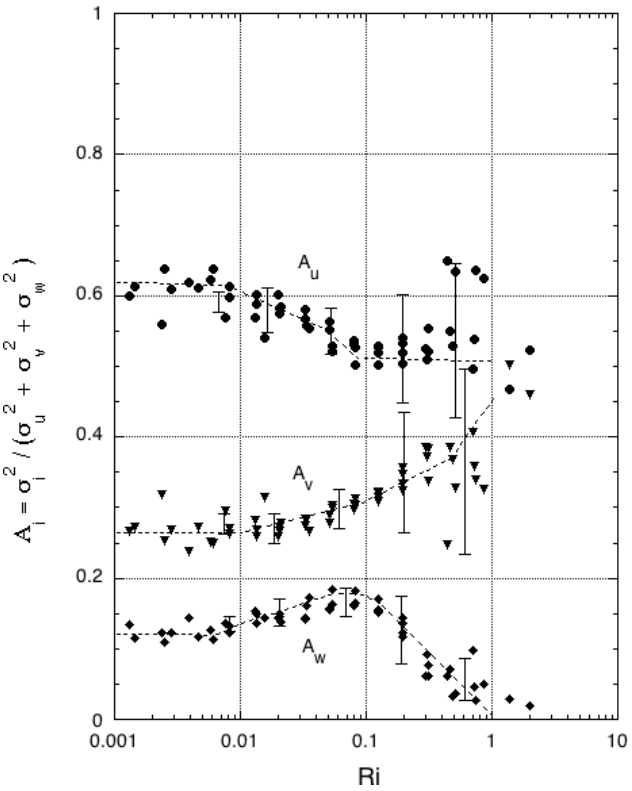

Figure 7. Dependence of the bin-averaged values of the dimensionless components of the doubled turbulent kinetic energy, $A_u = \sigma_u^2/q^2$, $A_v = \sigma_v^2/q^2$, $A_w = \sigma_w^2/q^2$, on the Richardson number *Ri*. The vertical lines represent the confidence intervals evaluated at level 5.

Copyright © 2010 Royal Meteorological Society

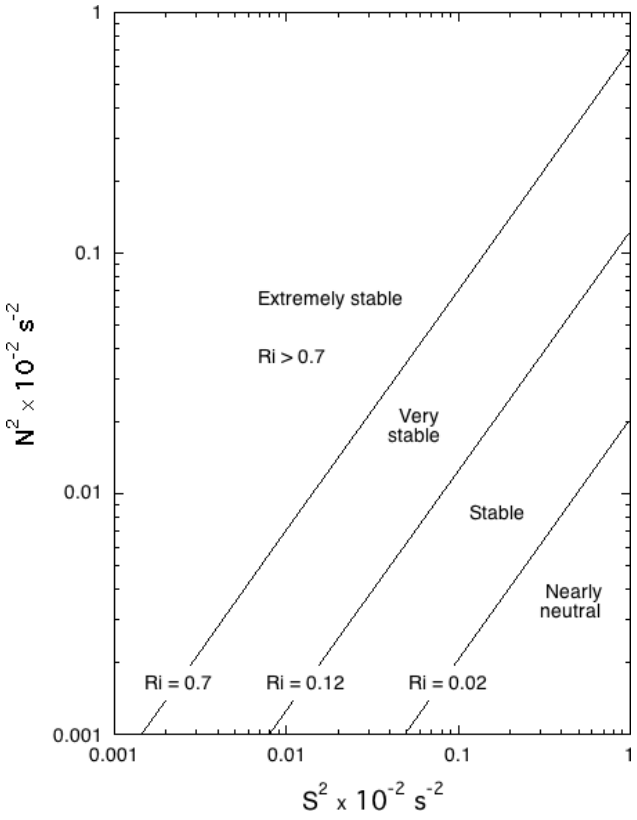

Figure 8. Sub-regimes of the stably stratified boundary layer.

The Prandtl number is 0.9 in nearly neutral conditions, and 0.7 for larger values of *Ri*. The negative correlation coefficient between the vertical velocity and the temperature, $-r_{w\theta}$, has a local maximum of about 0.39 at $Ri \approx 0.08$, and monotonically decreases at larger values of *Ri*. The dimensionless components of the doubled turbulent kinetic energy A_u and A_v have a tendency to become nearly equal for $Ri > 0.7$. The vertical component A_w reaches maximum at $Ri \approx 0.1$ and subsequently decreases for larger values of the Richardson number. The budget of the turbulent kinetic energy indicates that at the Richardson number $Ri > Ri_s = 0.7$, turbulence is non-stationary and decaying, or sporadic.

Stable turbulence can be classified into four sub-regimes: 'near neutral' regime for $0 < Ri < 0.02$, the 'stable' regime for $0.02 < Ri < 0.12$, the 'very stable' regime for $0.12 < Ri < 0.7$, and the 'extremely stable' regime for $Ri > 0.7$. In the nearly neutral regime, the master similarity functions follow the exact power laws. The stable regime is the transition between nearly neutral and stable conditions. In the very stable-continuous regime, the master similarity functions *G* can be described by empirical power laws. The generality of any scaling laws in extremely stable conditions is problematic. The specified regimes are controlled by a local stability parameter *Ri*, and thus can generally occur at any level within the stably stratified boundary layer.

Acknowledgements

The author's appreciation is directed to A. A. Grachev of CIRES/NOAA for providing the processed SHEBA data. The work has been partly supported by the National Science Foundation grant ATM-0938293.

References

Anderson PS. 2009. Measurement of Prandtl number as a function of Richardson number avoiding self- correlation. *Boundary-Layer Meteorol.* **131**: 345–362.
Andreas EL, Hill RJ, Gosz JR, Moore DI, Otto WD, Sarma AD. 1998. Statistics of surface-layer turbulence over terrain with metre-scale heterogeneity. *Boundary-Layer Meteorol.* **86**: 379–408.
Andreas EL, Fairall CW, Guest PS, Persson POG. 1999. 'An overview of the SHEBA atmospheric surface flux program.' Pp 550–555 in *Proceedings 13th Symposium on boundary layers and turbulence, Dallas, Texas*. Amer. Meteorol. Soc.
Andreas EL, Fairall CW, Grachev AA, Guest PS, Horst TW, Jordan RE, Persson POG. 2003. 'Turbulent transfer coefficients and roughness lengths over sea ice: The SHEBA results.' *Seventh Conference on polar meteorology and oceanography and Joint Symposium on high-latitude climate variations, 12–16 May 2003, Hyannis, Massachusetts*. Amer. Meteorol. Soc. AMS Preprint CD-ROM.
Andreas EL, Claffey KJ, Jordan RE, Fairall CW, Guest PS, Persson POG, Grachev AA. 2006. Evaluations of the von Kármán constant in the atmospheric surface layer. *J. Fluid Mech.* **559**: 117–149.
Baas P, Steeneveld GJ, van de Wiel BJH, Holtslag AAM. 2006. Exploring self-correlation in flux–gradient relationships for stably stratified conditions. *J. Atmos. Sci.* **63**: 3045–3054.
Barenblatt GI. 1996. *Scaling, self-similarity, and intermediate asymptotics. Cambridge Texts in Applied Mathematics* 14. Cambridge University Press.
Blackadar AK. 1962. The vertical distribution of wind and turbulent exchange in a neutral atmosphere. *J. Geophys. Res.* **67**: 3095–3102.
Esau IN, Grachev AA. 2007. Turbulent Prandtl number in stably stratified atmospheric boundary layer: Intercomparison between LES and SHEBA data. *e-WindEng* 006: 01–17. Available at http://ejournal.windeng.net.
Galperin B, Sukoriansky S, Anderson PS. 2007. On the critical Richardson number in stably stratified turbulence. *Atmos. Sci. Lett.* **8**: 65–69.
Grachev AA, Fairall CW, Persson POG, Andreas EL, Guest PS. 2005. Stable boundary-layer scaling regimes: The SHEBA data. *Boundary-Layer Meteorol.* **116**: 201–235.
Grachev AA, Andreas EL, Fairall CW, Guest PS, Persson POG. 2007a. SHEBA flux-profile relationships in the stable atmospheric boundary layer. *Boundary-Layer Meteorol.* **124**: 315–333.
Grachev AA, Andreas EL, Fairall CW, Guest PS, Persson POG. 2007b. On the turbulent Prandtl number in the stable atmospheric boundary layer. *Boundary-Layer Meteorol.* **125**: 329–341.
Grachev AA, Andreas EL, Fairall CW, Guest PS, Persson POG. 2008. Turbulent measurements in the stable atmospheric boundary layer during SHEBA: Ten years after. *Acta Geophys.* **56**: 142–166.
Klipp CL, Mahrt L. 2004. Flux-gradient relationship, self-correlation and intermittency in the stable boundary layer. *Q. J. R. Meteorol. Soc.* **130**: 2087–2103.
Kolmogorov AN. 1941. Energy dissipation in locally isotropic turbulence. *Doklady AN SSSR* **32**(1): 19–21.
Kukharets VP, Tsvang LR. 1998. Atmospheric turbulence characteristics over a temperature- inhomogeneous land surface. Part I: Statistical characteristics of small-scale spatial inhomogeneities of land surface temperature. *Boundary-Layer Meteorol.* **86**: 89–101.
Monin AS, Obukhov AM. 1954. Basic laws of turbulence mixing in the surface layer of the atmosphere. *Trudy Geofiz. Inst. AN SSSR.* **24**: 163–187.
Nieuwstadt FTM. 1984. The turbulent structure of the stable, nocturnal boundary layer. *J. Atmos. Sci.* **41**: 2202–2216.
Ohya Y. 2001. Wind-tunnel study of atmospheric stable boundary layers over a rough surface. *Boundary-Layer Meteorol.* **98**: 57–82.
Persson POG, Fairall CW, Andreas EL, Guest PS, Perovich DK. 2002. Measurements near the Atmospheric Surface Flux Group tower at SHEBA: Near-surface conditions and surface energy budget. *J. Geophys. Res.* **107**: 8045, DOI:10.1029/2000JC000705.
Prandtl L. 1932. Meteorologische Anwendungen der Strömungslehre. *Beitr. Phys. Atmos.* **19**: 188–202.
Sorbjan Z. 1986a. On similarity in the atmospheric boundary layer. *Boundary-Layer Meteorol.* **34**: 377–397.
Sorbjan Z. 1986b. On the vertical distribution of passive species in the atmospheric boundary layer. *Boundary- Layer Meteorol.* **35**: 73–81.
Sorbjan Z. 1988. Structure of the stably-stratified boundary layer during the SESAME-1979 experiment. *Boundary-Layer Meteorol.* **44**: 255–260.
Sorbjan Z. 1989. *Structure of the atmospheric boundary layer*. Prentice-Hall.
Sorbjan Z. 2006a. Local structure of turbulence in stably stratified boundary layers. *J. Atmos. Sci.* **63**: 1526–1537.

Copyright © 2010 Royal Meteorological Society

Sorbjan Z. 2006b. Comments on 'Flux-gradient relationship, self-correlation and intermittency in the stable boundary layer'. *Q. J. R. Meteorol. Soc.* **132**: 1371–1373.
Sorbjan Z, Balsley BB. 2008. Microstructure of turbulence in the stably stratified boundary layer. *Boundary-Layer Meteorol.* **129**: 191–210.
Sorbjan Z, Grachev AA. 2010. An evaluation of the flux-gradient relationship in the stable boundary layer. *Boundary-Layer Meteorol.* **135**(3): 385–405.
Tsvang LR, Kukharets VP, Perepelkin VG. 1998. Atmospheric turbulence characteristics over a temperature-inhomogeneous land surface. Part II: The effect of small-scale inhomogeneities of surface temperature on some characteristics of the atmospheric surface layer. *Boundary-Layer Meteorol.* **86**: 103–124.
Zilitinkevich SS, Elperin T, Kleeorin N, Rogachevskii I. 2007. Energy- and flux-budget (EFB) turbulence closure model for stably stratified flows. Part I: Steady-state, homogeneous regimes. *Boundary-Layer Meteorol.* **125**: 167–191.

Copyright © 2010 Royal Meteorological Society